JACC: CLINICAL ELECTROPHYSIOLOGY VOL. 7, NO. 7, 2021

CLINICAL ELECTROPHYSIOLOGY - MAPPING

Evaluation of Directed Graph-Mapping in Complex Atrial Tachycardias

Enid Van Nieuwenhuyse, MSc,[a,*] Teresa Strisciuglio, MD,[b,c,*] Giuseppe Lorenzo, MSc,[d] Milad El Haddad, PhD,[b] Jan Goedgebeur, PhD,[e,f] Nico Van Cleemput, PhD,[e] Christophe Ley, PhD,[e] Alexander V. Panfilov, PhD,[a,g,h] Jan de Pooter, PhD, MD,[b,i] Yves Vandekerckhove, MD,[b] Rene Tavernier, PhD, MD,[b] Mattias Duytschaever, PhD, MD,[b,i] Sebastien Knecht, PhD, MD,[b] Nele Vandersickel, PhD[a]

ABSTRACT

OBJECTIVES Directed graph-mapping (DGM) is a novel operator-independent automatic tool that can be applied to the identification of the atrial tachycardia (AT) mechanism. In the present study, for the first time, DGM was applied in complex AT cases, and diagnostic accuracy was evaluated.

BACKGROUND Catheter ablation of ATs still represents a challenge, as the identification of the correct mechanism can be difficult. New algorithms for high-density activation mapping (HDAM) render an easier acquisition of more detailed maps; however, understanding of the mechanism and, thus, identification of the ablation targets, especially in complex cases, remains strongly operator-dependent.

METHODS HDAMs acquired with the latest algorithm (COHERENT version 7, Biosense Webster, Irvine, California) were interpreted offline by 4 expert electrophysiologists, and the acquired electrode recordings with corresponding local activation times (LATs) were analyzed by DGM (also offline). Entrainment maneuvers (EM) were performed to understand the correct mechanism, which was then confirmed by successful ablation (13 cases were centrifugal, 10 cases were localized re-entry, 22 cases were macro-re-entry, and 6 were double-loops). In total, 51 ATs were retrospectively analyzed. We compared the diagnoses made by DGM were compared with those of the experts and with additional EM results.

RESULTS In total, 51 ATs were retrospectively analyzed. Experts diagnosed the correct AT mechanism and location in 33 cases versus DGM in 38 cases. Diagnostic accuracy varied according to different AT mechanisms. The 13 centrifugal activation patterns were always correctly identified by both methods; 2 of 10 localized reentries were identified by the experts, whereas DGM diagnosed 7 of 10. For the macro-re-entries, 12 of 22 were correctly identified using HDAM versus 13 of 22 for DGM. Finally, 6 of 6 double-loops were correctly identified by the experts, versus 5 of 6 for DGM.

CONCLUSIONS Even in complex cases, DGM provides an automatic, fast, and operator-independent tool to identify the AT mechanism and location and could be a valuable addition to current mapping technologies.

From the [a]Department of Physics and Astronomy, Ghent University, Ghent, Belgium; [b]Cardiology Department, AZ Sint-Jan, Bruges, Belgium; [c]Department of Advanced Biomedical Sciences, University of Naples Federico II, Naples, Italy; [d]Biosense Webster Inc., Irvine, California, USA; [e]Department of Applied Mathematics, Computer Science and Statistics, Ghent University, Ghent, Belgium; [f]Computer Science Department, University of Mons, Mons, Belgium; [g]Laboratory of Computational Biology and Medicine, Ural Federal University, Ekaterinburg, Russia; [h]Arrhythmia Department, Almazov National Medical Research Centre, Saint Petersburg, Russia; and the [i]Ghent University Hospital Heart Center, Ghent University, Ghent, Belgium. *Mrs. Van Nieuwenhuyse and Dr. Strisciuglio contributed equally to this work and are joint first authors.

ISSN 2405-500X https://doi.org/10.1016/j.jacep.2020.12.013

Ablation of atrial tachycardias (AT) remains challenging despite recent improvements in mapping technologies (1–3). New, high-density activation (HDA) mapping systems using velocity vectors enable the visualization of atrial activation wavefronts, facilitating the identification of potential circuits and foci responsible for the AT. However, these systems have limitations: 1) they often suggest more than 1 potential activation route; and 2) the wrong automatic annotation of low voltage and fractionated potentials can render confusing activation maps (4). Very recently directed graph-mapping (DGM), a novel automatic technique based on the creation of a directed network to represent the cardiac excitation, was introduced (5). DGM has been tested using in-silico data and retrospective data from 31 relatively simple cases of regular AT. DGM has shown to be effective in detecting the mechanism and the precise circuit of such ATs automatically and instantaneously. The next logical step is to apply this methodology to more complex AT cases, where operator identification of the mechanisms would be essential. Thus, the present study evaluated the diagnostic accuracy of DGM in complex right and left ATs by comparing the automatic diagnoses generated by DGM with, first, the diagnoses made by the consensus of 4 expert electrophysiologists (EPs) based on the interpretation of HDA maps, and second, the final diagnosis as confirmed by additional entrainment maneuvers (EM) and ablation (EM+ablation).

SEE PAGE 950

METHODS

STUDY DESIGN. Between March 2018 and February 2019, consecutive patients undergoing ablation of symptomatic ATs with the exclusion of isolated common flutter at AZ Sint-Jan Bruges Hospital were enrolled in the study. Cases were included if the left or right atrium mapping density included >300 activation points per screened chamber and if the EM were performed. The HDA map was first analyzed offline by 4 expert EPs blinded to the final diagnosis and then by DGM. A comparison was made, with additional results from EM and ablation (EM+ablation). Patients' informed consent and a detailed case report form of the procedure were collected in a local database. The study is was conducted in accordance with the Declaration of Helsinki and was approved by the local Ethics Committee.

ABLATION PROCEDURE AND HIGH-DENSITY ACTIVATION MAPPING. All procedures were performed by 4 different EPs with the patient under general anesthesia and receiving direct anticoagulants (last dose: <24 h before the procedure) or uninterrupted warfarin therapy. Antiarrhythmic drugs were withdrawn 24 h before the procedure. No antiarrhythmic medication was administered during the procedure. An esophageal temperature monitoring probe (SensiTherm, St. Jude Medical, Abbott, Chicago, Illinois) was placed at the discretion of the operator. Intravenous heparin was administered after thee femoral vein was accessed to achieve an activated clotting time of >350 s. A decapolar coronary sinus catheter was introduced through the right femoral vein. For left-sided AT a double-transseptal puncture was performed with conventional long sheaths (model SL0, St. Jude Medical, Abbott, Chicago, Illinois). A multielectrode mapping catheter (PENTARAY, Biosense Webster Inc., Irvine, California) and an open-tip irrigated radiofrequency catheter (8-F) with tip-integrated contact force sensor (Thermocool SmartTouch, Biosense-Webster, Irvine, California) were positioned in the left atrium (LA) or right atrium (RA). Then, calibration of the contact force catheter, respiratory gating, and acquisition of the 3D geometry of the LA/RA (CARTO System, Biosense Webster) were performed. Automated and continuous acquisition of local activation time (LAT) points was performed with the CONFIDENSE mapping module (CARTO, Biosense Webster). Furthermore the LAT maps were analyzed using the COHERENT module (CARTO, Biosense Webster), which has been previously described (6). This new algorithm takes into account 3 descriptors: the LAT value, conduction vector, and the probability of nonconductivity. Those 3 descriptors are used to generate an integrative activation map displayed as a vector map. The

ABBREVIATIONS AND ACRONYMS

AF = atrial fibrillation
AT = atrial tachycardia
CS = coronary sinus
CTI = cavotricuspid isthmus
DGM = directed graph-mapping
EM = entrainment mapping
EP = electrophysiologist
HDAM = high-density activation map
LA = left atrium
LAT = local activation time
LPV = left pulmonary vein
MV = mitral valve
PPI-TCL = post-pacing interval-tachycardia cycle length
RA = right atrium
RPV = right pulmonary vein

The authors attest they are in compliance with human studies committees and animal welfare regulations of the authors' institutions and Food and Drug Administration guidelines, including patient consent where appropriate. For more information, visit the Author Center.

Manuscript received August 4, 2020; revised manuscript received December 14, 2020, accepted December 16, 2020.

JACC: CLINICAL ELECTROPHYSIOLOGY VOL. 7, NO. 7, 2021
JULY 2021:936–49

FIGURE 1 Workflow of DGM

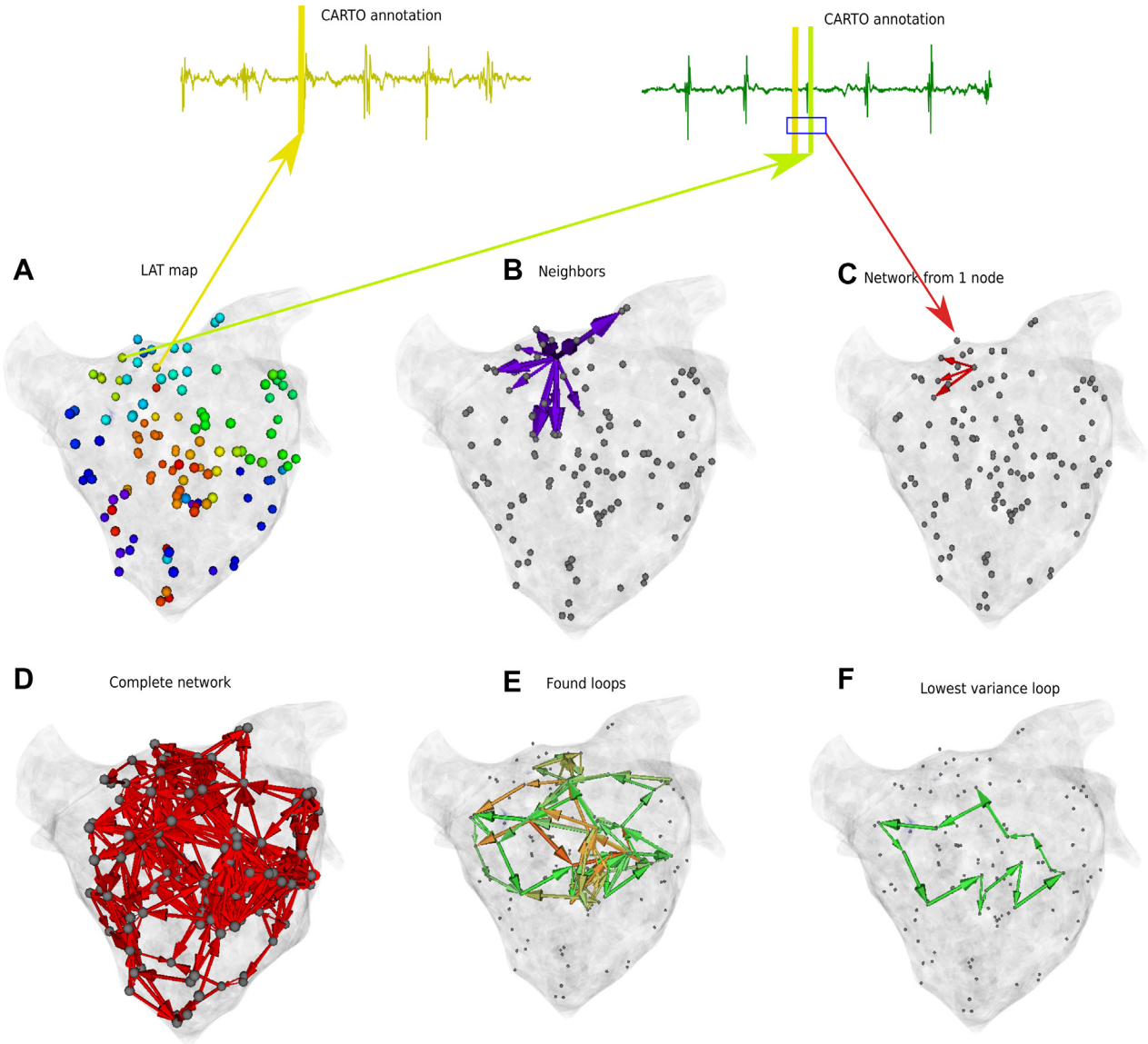

(A) First, the annotated points with corresponding LAT values are loaded. **(B, C)** Second, for each node, neighbors were determined, and an **arrow** is drawn in case the difference in LATs values of 2 neighbors and their corresponding distances are within the considered velocities. **(D)** Then, the network is created for each node and merge. **(E)** Afterward, the cycles are detected, and **(F)** the ones with the highest variance are considered responsible for the AT. AT = atrial tachycardias; DGM = directed graph-mapping; LAT = local activation time.

algorithm then identifies the optimal conduction mechanism, considering physiological barriers manifested by scar and double potentials. The coloring is based on the best-fit solution of all LAT values of the map, identifying the conduction mechanism.

INTERPRETATION OF HDA MAPS. The HDA maps were shown offline to 4 expert EPs. A consensus on the mechanism and AT route and origin was reached unless they considered the map "non-univocally interpretable." The classification nonunivocally interpretable included the cases where the experts did not agree on the mechanism or the cases where the mechanism was completely unknown.

DIRECTED GRAPH-MAPPING. Directed graph-mapping (DGM) is a novel technique based on the concepts of network theory. DGM makes use of the annotated

TABLE 1 Patient Clinical Characteristics

Males	31 (72)
Age, yrs	69 (62 ± 74)
$CHAD_2VASc$ score	2.2 to −1.5
AADs class 1c	3 (7)
Sotalol	7 (17)
Amiodarone	3 (7)
No AADs	4 (13)
Anti-vitamin K	7 (17)
OAC	27 (64)
No AC	6 (14)
Median number of previous ablations	1 (1-2)

Values are n (%), median (mean ± SD), or median (interquartile range).

AC = anticoagulants; AAD = antiarrhythmic drugs; $CHAD_2VASc$ = congestive heart failure, hypertension, age ≥75 years, diabetes mellitus, stroke or transient ischemic attack [TIA], vascular disease, age 65 to 74 years, sex category; OAC = oral anti-coagulants.

LATs as given by the current available mapping system and the corresponding XYZ coordinates of these LATs within the heart geometry, which are also created by means of the current available mapping system (**Figure 1A**). As described in the study by Vandersickel et al. (5), the following network was constructed. First, for a given electrode, its neighbors were determined (**Figure 1B**). Then, for each pair of neighbors, the 2 electrodes were connected by a directed arrow if and only if their velocities (the distance between the 2 electrodes divided by the difference in LAT) lay between predefined minimal and maximal conduction velocities. For all cases, the minimal conduction velocity varied between 0.1 and 0.25 mm/ms in steps of 0.05 mm/ms. The maximal conduction velocity was always fixed to a maximum of 2.0 mm/ms. In **Figure 1C**, the arrows for a single electrode are shown. Repeating this step for all electrodes, a directed network was obtained representing the cardiac excitation created from the LAT maps (**Figure 1D**). Because the minimally allowed conduction velocity puts a restriction on the allowed arrows drawn in the directed graph, this process was iterated over the multiple minimal conduction velocities. At each minimal conduction velocity, the directed network was created, and rotational activity, either localized or macro-re-entrant circuits, were found by detection of the directed cycles in the network (**Figure 1E**). At each iteration, detected cycles are collected based on their geometrical centers into clusters. In case the geometrical center of 2 cycles lay apart by more than 15 mm, the cycles are considered to belong to a different cluster. In case no cycles were found, the DGM tool was automatically activated to look for source nodes, that is, the collectives of nodes with only outgoing arrows (5). For this study, an additional feature was added to the protocol to improve the algorithm and fully automate the DGM tool (7). This feature is called "phase variance" and is a mathematical construct which represents the regularity of the cycles detected in the constructed network of the AT. The cycles with the lowest variance correspond to concentric cycles around the obstacle, valve, or excitable tissue responsible for re-entry. Cycles were considered potentially relevant for diagnosis only if: 1) they have more than 8 arrows; and 2) the phase variance of the cycle is the lowest found in its cluster. For each cluster, the cycle with the lowest variance was considered. Afterward, a cutoff variance, based on simulations, was applied, and only the clusters with a minimal variance between the range of the lowest found variance to the lowest found variance (p + 0.15) are considered for interpretation and visualization on the geometry of the atria. The loops fitting this criteria are shown (**Figure 1F**). Crossloops are loops in which the arrows of the loop intersect each other, and loops with fewer than 8 arrows were never taken into account because they did not appear to properly represent the cardiac excitation. It is explicitly noted that this program was tested and optimized for complex AT on the gathered database and, hence, was an offline procedure in this study. However, for future studies, DGM can also be used as an online tool to analyze the arrhythmia during the procedure. Even if DGM depends on the annotated signals of the CARTO module, there are some significant differences between the COHERENT module and DGM. DGM provides an automated diagnosis, in a way that the circuit of the AT is projected onto the atrial geometry. The EP needs only to determine optimized ablation location for given projected circuit which is in contrast with the COHERENT module showing local velocity arrows pointing toward what is hinted at as the direction of the electrical propagation of the excitation front. These arrows still need to be interpreted by the EP to obtain the final diagnosis. Therefore, the final diagnosis can still be different depending on the interpretation of the EP.

FINAL ATRIAL TACHYCARDIA DIAGNOSIS AND ABLATION. The final AT mechanism was based on the results obtained by using the HDA map in combination with EM with additional confirmation by ablation (referred to as high-density activation mapping [HDAM] +EM+ablation, or the gold standard). Entrainment was performed at a cycle length of 10 ms less than the tachycardia cycle length (TCL). A postpacing interval (PPI) not exceeding the TCL by more than 30 ms in 3 opposite atrial locations corroborated the diagnosis of macro-re-entry. A color code was used to illustrate the PPI results: a green point

TABLE 2 AT Mechanisms and Characteristics*

AT Mechanism	TCL	HDAM Points
Breakthrough or focal (n = 13)	290 (246-350)	786 (487-1,065)
Single loop ATs (n = 22)	285 (243-316)	778 (539-1,064)
Roof circuits (n = 11)		
Approximate LPVs (n = 3)	290 (244-300)	1359 (773-1,020)
Approximate RPVs (n = 8)	283 (222-301)	772 (553-974)
Perimitral circuits (n = 10)	300 (283-269)	670 (424-1,090)
CTI-dependent (n = 1)	260	2,737
Double loop ATs (n = 6)	250 (239-269)	937 (431-1,337)
Localized re-entries (n = 10)	296 (255-370)	877 (413-1,600)

Values are n (% range). *The mean TCL and amount of HDAM points is shown. The range of corresponding values within the considered categories is shown in parentheses.

AT = atrial tachycardias; HDAM = high-density activation mapping; LPV = left pulmonary vein; RPV = right pulmonary vein; TCL = tachycardia cycle length.

corresponded to a PPI-TCL of <30 ms; a yellow point to a PPI-TCL between 30 and 50 ms; and a black point to a PPI-TCL of >50 ms. The diagnosis of the AT mechanism was considered correct if the AT terminated during radiofrequency ablation to sinus rhythm or to another AT. Another AT was defined by the change in TCL and change in the activation pattern. Radiofrequency ablation (20-45 W, 30-cm^3 irrigation rate) was performed depending on the AT mechanism. In every procedure, the endpoint was the termination of the tachycardia during ongoing ablation, and the operators aimed to reach the non-inducibility of any AT at the end of the procedure. The inducibility protocol consisted of a burst of 10 consecutive paced beats from the proximal coronary sinus, with the fastest pacing rate resulting in 1:1 capture and with a minimum cycle length of 200 ms. In patients who previously underwent pulmonary vein isolation, complete electrical isolation of all pulmonary veins was ensured before the end of the procedure, and additional ablation was performed, if required. If linear lesions were deployed and gaps were discovered, further ablation was undertaken in paced or sinus rhythm until bidirectional blockage was ascertained.

AT MECHANISM DEFINITIONS AND SITES OF ABLATION. Macro-re-entry was defined as an activation encircling a "large" central obstacle of several centimeters in diameter. For the LA, macro-re-entries were defined as roof-dependent circuits when turning around the right pulmonary veins (RPV) or left pulmonary veins (LPV), or perimitral when turning around the mitral valve (MV). For the RA, macro-re-entries were classified as circuits that were cavo-tricuspid isthmus (CTI)-dependent or as circuits around a spontaneous or iatrogenic scar. A double-loop AT was defined as 2 simultaneous macro-re-entry circuits with a common isthmus. For the termination of macro-re-entries, the operators performed a linear ablation to interrupt the circuit, and they ablated until a bidirectional block was reached. In the case of double-loop re-entries, linear ablation was not performed at the common isthmus but at another isthmus location to allow confirmation of the double-loop mechanism (linear ablation would terminate 1 of both circles, with subsequent change in EM). Localized re-entries were defined by the presence of the following criteria: 1) electrograms covering ≥75% of the cycle length of the AT within an area (<2-3 cm) covering a single segment or 2 contiguous segments; 2) a PPI <30 ms at the site; 3) an identifiable zone of slow conduction; and 4) centrifugal activation of the atrium from the area (8,9). In case of a localized re-entry, the ablation was focused mostly on the earliest area where local low-amplitude and long duration electrogram filled >75% of the TCL. A focal AT due, for example, to automaticity or triggered activity, was defined as (1) a radial spread in all directions from a single site of earliest activation indicated by CARTO activation and propagation map; or (2) a range of activation duration less than the tachycardia cycle length (10). In that case, ablation was performed at the origin of the activation, where the unipolar electrogram demonstrated a QS configuration with a steep negative deflection preceding the P wave. In the case of a focal pattern located at the septum of the LA, the map was also classified within the category of centrifugal activation patterns. However, these could theoretically correspond to a passive LA activation from a right-sided AT (breakthrough) or a real septal focal mechanism (focal). In that case, where centrifugal activation was located at the septum of the LA, the activation mapping of the RA also was performed to confirm or exclude the origin from a right-sided AT.

STATISTICS. Continuous variables are presented in the tables as mean ± standard deviation (SD) or as median with interquartile range (IQR). Categorical variables are presented as percentages (%) and counts. A statistical test was performed to compare the results of DGM with those of the HDAM, to determine whether 38 of 51 correct analyses improved significantly on the 33 of 51 correct diagnoses from the experts. A variant of the McNemar test was used for paired nominal data, namely, if the differences between the number of cases where DGM was correct and the experts were incorrect (8 cases) and the number of cases where the opposite held (3 cases) is significantly different from 0 (here, larger than 0).

FIGURE 2 **Results of HDAM and DGM Compared to HDAM Plus EM Plus Ablation**

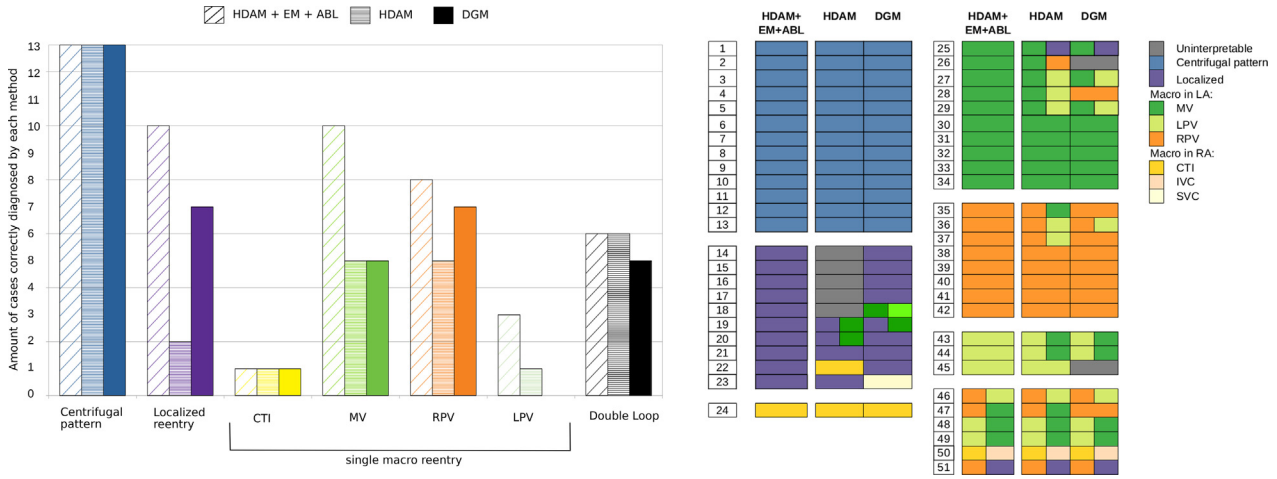

Frame 1 shows the distribution of HDAM+EM+ablation diagnosed cases per category. Alongside of these results, the correctly diagnosed cases by HDAM and DGM are presented. In the inline frame the specific diagnosis of each separate case is visualized. Results are represented based on HDAM + EM + ablation (EM, **first column**), HDA interpretation (HDAM, **middle column**) and DGM detected diagnosis (DGM, **right column**). If more than 1 circuit was found for a certain case, the **column** was divided according to the number of circuits. DGM = directed graph-mapping; EM = entrainment maneuvers; HDA = high-density activation; HDAM = high-density activation mapping.

This test is therefore based on a binomial distribution with size 8 + 3 = 11 and success rate (under the null hypothesis of no difference) of one-half. We refer to the Results section below for the outcome of this test.

RESULTS

STUDY POPULATION AND PROCEDURAL CHARACTERISTICS. A total of 51 ATs from 40 consecutive patients were analyzed using HDAM and automated DGM. Results from either mapping technology were compared with the final diagnosis confirmed with HDAM+EM+ablation. Clinical characteristics of the patients are reported in **Table 1**. Overall, 44 LA maps and 7 RA maps were recorded and analyzed. The median TCL was 290 (IQR: 246 to 350), whereas the median number of points acquired per map was 786 (IQR: 487 to 1,065) (**Table 2**).

GOLD STANDARD: AT DIAGNOSIS BY HDAM + EM + ABLATION. The 51 AT cases were diagnosed with HDAM+EM, and based on it, ablation was performed. In all cases ablation confirmed the HDAM+EM diagnosis and, thus, was considered the "gold standard," to which the other diagnostic methods were compared. The excitation patterns were divided into the following categories. In total, 13 centrifugal excitation patterns were detected, from which 3 focal sources and 10 passive septal centrifugal patterns (a passive activation from a right sided AT). Ten localized re-entries were diagnosed, and the distribution of their location in both LA and RA is illustrated in Supplemental Figure S1. A total of 22 single macro-reentrant circuits were found. Among those circuits were 1 CTI flutter, 10 re-entries around the MV, 8 roof-dependent re-entries around the RPV, and 3 roof-dependent re-entries around the LPVs. Finally 6 double-loop re-entries were found: 1 case where the excitation pattern was driven by a localized re-entry in combination with a macro re-entry and 5 cases where the AT was driven by 2 macro re-entries simultaneously. The distribution of the HDAM+EM+ablation-diagnosed cases is presented in **Figure 2**, left panel, together with diagnosis obtained using HDAM as well as DGM, as discussed below.

ACCURACY OF DGM COMPARED TO THE ACCURACY OF THE GOLD STANDARD. This section discusses the overall performance of DGM compared to the gold standard according to category (**Figure 2**, left panel). In **Figure 2**, right panel, additional data are provided on a case-by-case basis.

Centrifugal patterns. As shown in **Figure 2**, left panel, all 13 centrifugal activation patterns (10 passive centrifugal activation due to right sided AT +3 focal) were correctly identified by DGM, resulting in a 100% success rate for centrifugal excitation patterns.

FIGURE 3 A Case of Localized Re-Entry

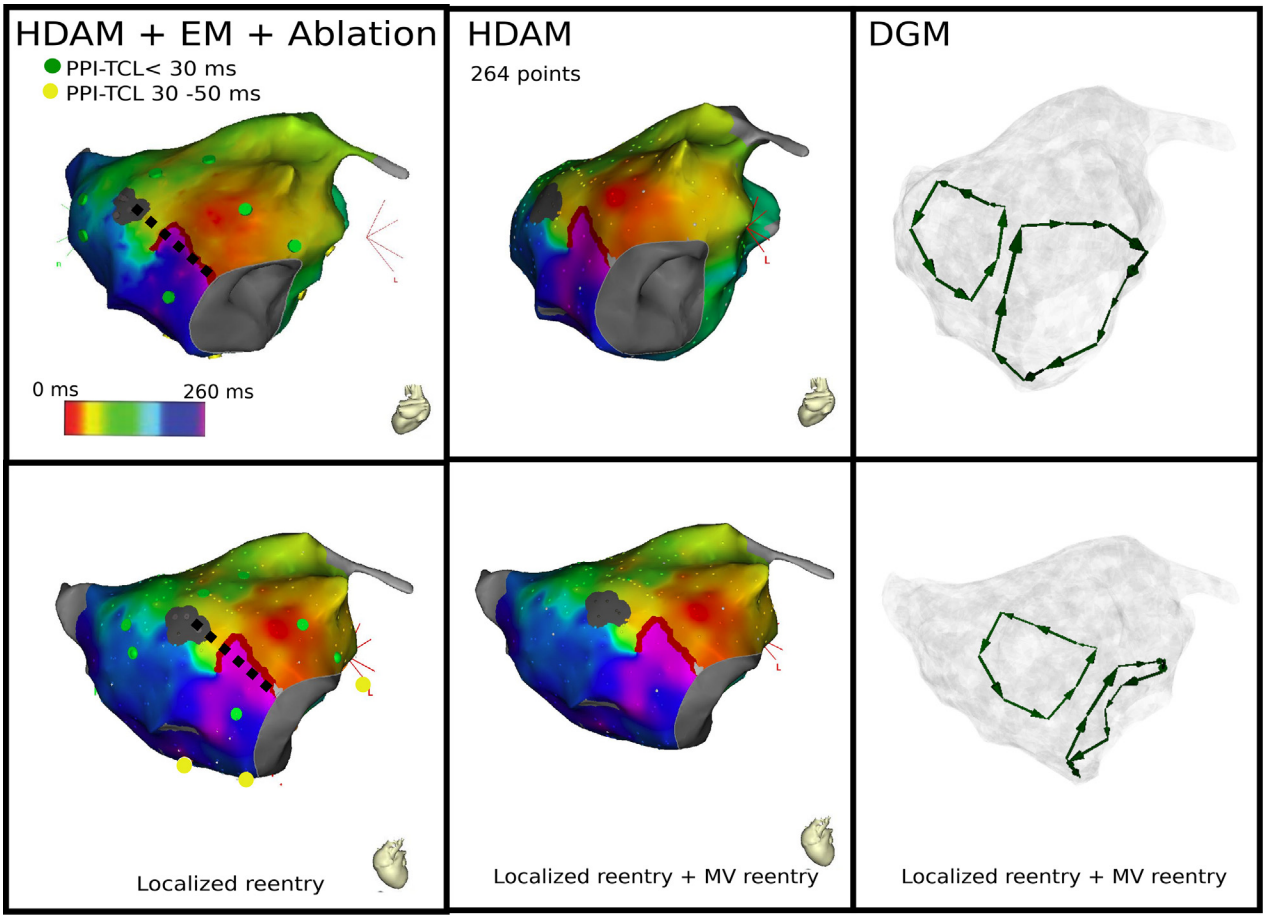

This figure represents case 19. Shown is the HDAM+EM+ablation, confirming the diagnosis of a localized re-entry around an anterior scar and the performance of HDAM and DGM. **(Upper panel)** Left anterior oblique view. **(Lower panel)** Anteroposterior view of the LA is shown. In addition to the localized re-entry, the 4 experts identified a perimitral circuit (HDAM, **middle column**). Also, DGM **(right column)** found these 2 circuits. However, as can be seen in the **first column**, the **yellow dots**, representing a PPI-TCL difference of 30 to 50 ms, this MV circuit is excluded from the true mechanism. DGM = directed graph-mapping; EM = entrainment maneuvers; HDAM = high-density activation mapping PPI-TCL = PPI-TCL = post-pacing interval-tachycardia cycle length.

Single localized re-entries. From 10 confirmed cases of a single localized re-entry, 7 were correctly detected by DGM. However, in 3 cases, DGM resulted in a different diagnosis. In case 23 (Figure 2, right panel), DGM found a superior vena cava macro re-entry instead of the by HDAM+EM+ABL confirmed localized re-entry. In case 18 (Figure 2) the localized re-entry at the anterior wall was not found, but a double-loop circuit around MV and LPV was found instead. For case 19, although a localized re-entry at the anterior wall was correctly identified, an additional loop around the MV was found. Note, however, that the conclusion on the absence of this additional loop around MV is not straightforward. It can be seen from the left column in Figure 3, showing the PPI-TCL points colored according to their delay time and superimposed on the LAT map. The right column shows the rotation loops identified by DGM. Although green points are seen (points with a PPI-TCL difference less than 30 ms) around the scar, in the in Figure 3, upper left panel, a green PPI was seen close the MV, indicating that that part of the MV can also be in the rotation circuit. However, in Figure 3, lower left panel we also see multiple yellow points around the MV, indicating a PPI-TCL difference between 30 and 50 ms. Due to that, the rotation around MV was excluded as a true rotation circuit. Note, however, that such longer delay might

FIGURE 4 **A Case of Macro Re-Entry**

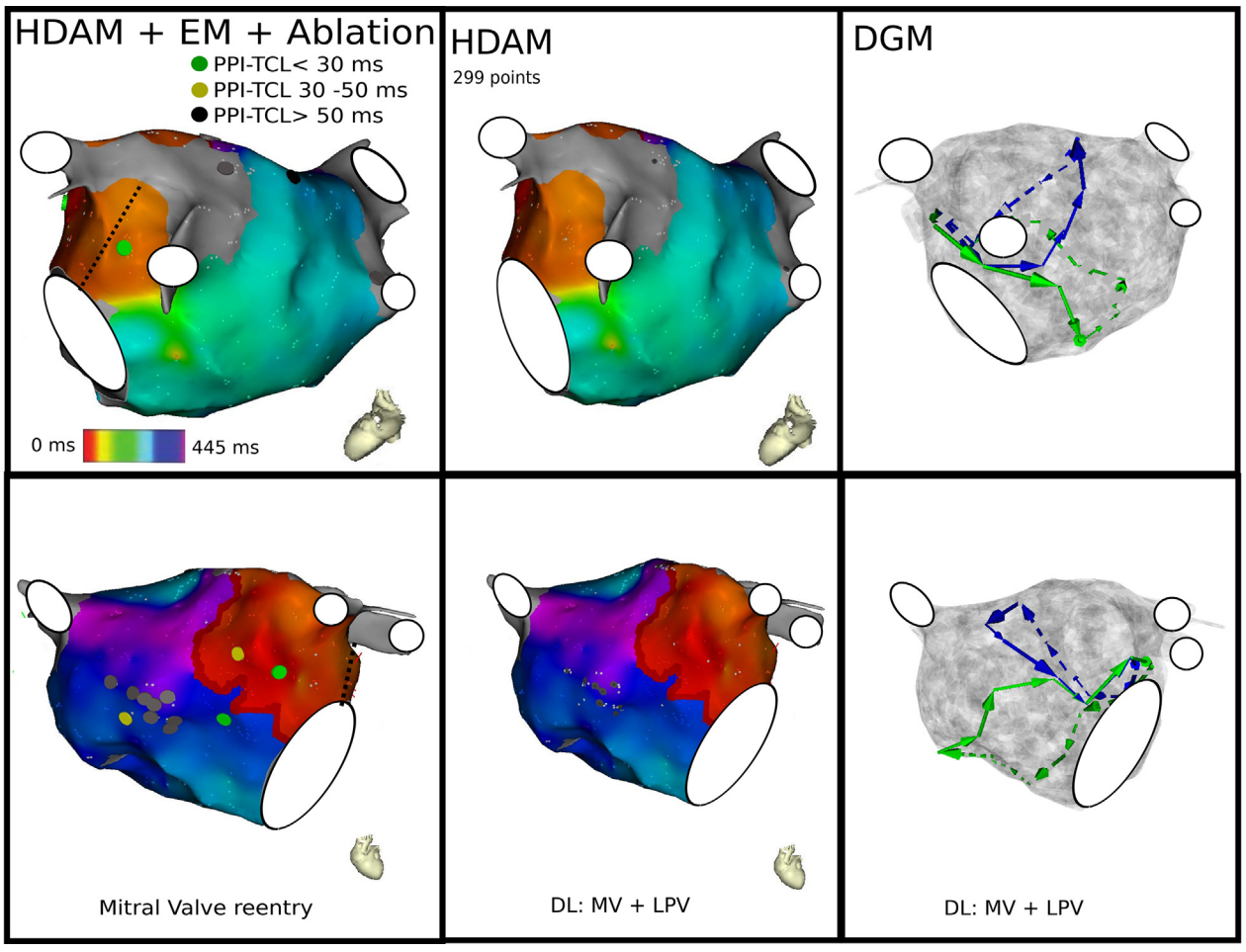

This figure represents case 27. The HDAM+EM+ablation confirmed the diagnosis of mitral valve re-entry and the performance of HDAM and DGM. **(Upper panel)** Left lateral view of LA is shown. **(Lower panel)** Anteroposterior view of LA. Although only a MV re-entry was the driving source, both HDAM as DGM analyzed an additional loop around the LPV. DGM = directed graph-mapping; EM = entrainment maneuvers; HDAM = high-density activation mapping; LA = left atrium; LPV = left pulmonary vein.

be also caused by slow local propagation, and interpretation of such PPI-TCL map was not straightforward. Anyway, counting or not counting MV rotation as macro re-entry circuit along the scar related re-entry resulted in the same ablation strategy: a lesion from the anterior wall scar tissue to the MV (Figure 3, left panels. dashed closed line). Overall DGM was correct in 7 of 10 (70%) for the localized re-entries.

Single macro re-entries. During AT, macro-re-entries occurred around the CTI, MV, RPV, and LPV. Of 51 cases, single macro re-entries were observed in 24 cases and from those cases, 21 were correctly identified by DGM.

We observed a CTI-dependent flutter only in 1 case, and it was correctly identified by DGM.

Of 10 re-entries solely around MV, 5 were correctly diagnosed by DGM. In the other 5 cases, DGM reported a different diagnosis. In 3 cases, an additional loop was detected: localized re-entry at the anterior wall (Figure 2, case 25) and 2 LPV macro-re-entries (Figure 2, cases 27 and 29). One such example is shown in Figure 4. Here the endpoints of LPVs and RPVs are visualized by the small white circles. HDAM+EM+ablation identified an MV macro-re-entry (Figure 4, left column). The right column (Figure 4) shows the 2 best variance loops found by DGM with the blue one indicating rotation

FIGURE 5 A Case of a Double-Loop

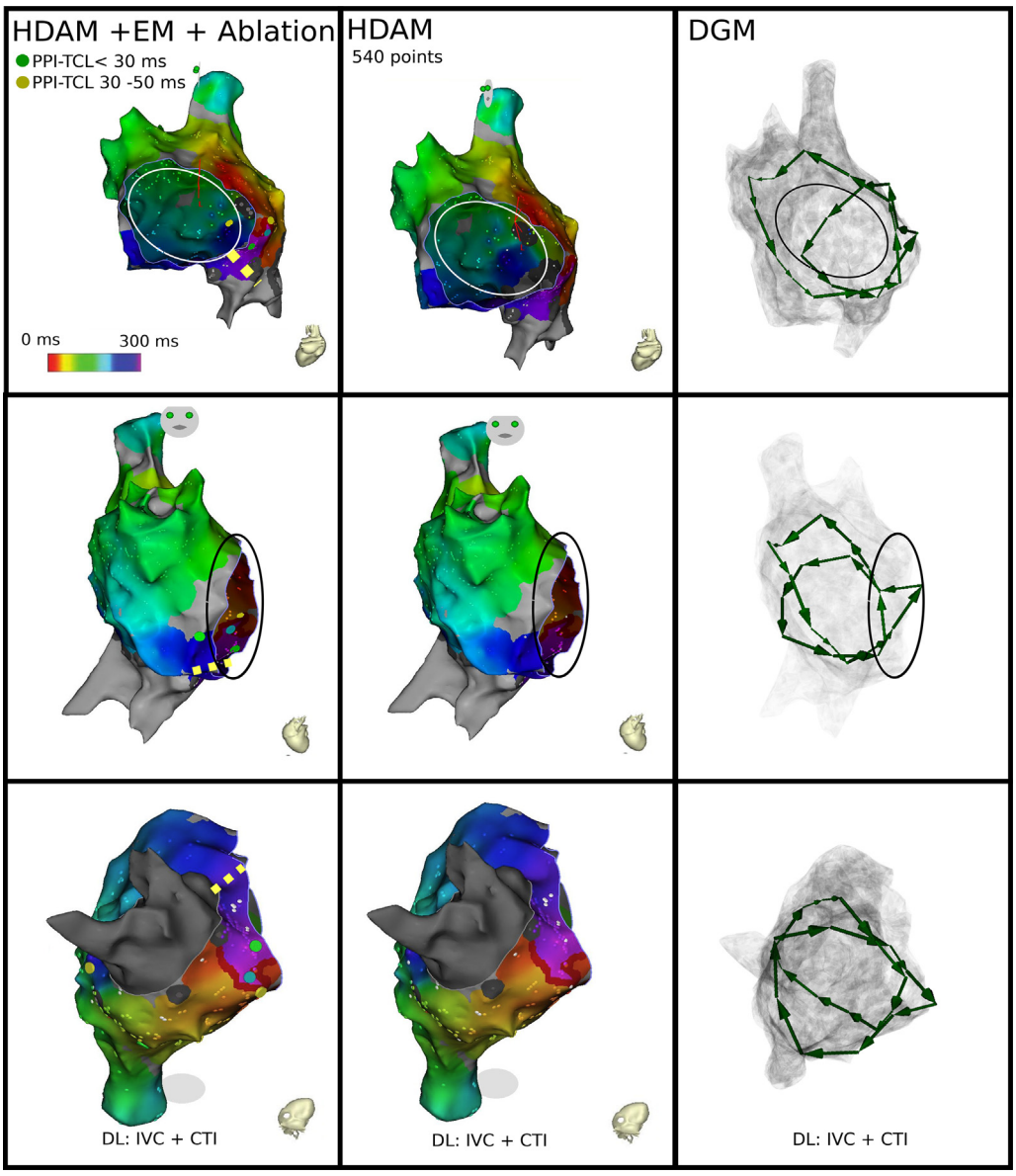

The figure represents case 50. The HDAM+EM+ablation diagnosed double-loop around IVC as well as CTI with the performance of HDAM and DGM. In the upper panel the left anterior oblique view of RA is shown and in the middle panel the right anterior oblique view of the RA. In the lower panel a view of the inferior is shown. Both systems correctly identified this diagnosis. CTI = cavotricuspid isthmus; DGM = directed graph mapping; HDAM = high-density activation mapping; IVC = inferior vena cava; RA = right atrium.

around the LPVs and the green one rotating around the MV. Note that, although the green loop does not follow the MV boundary, it can be continuously deformed to it along the atrial surface; thus, it corresponds to an MV rotation. The blue and green loops have a common isthmus as the ablation target. However DGM (as well as HDAM) suggests an additional ablation target (a roofline). Ablation at the mitral isthmus (Figure 4, dashed closed line in the left column) restored sinus rhythm. In case number 28 (Figure 2, right panel), instead of MV rotation, DGM found a re-entry around the inferior RPV and 1 case (Figure 2, right panel) was completely uninterpretable.

Of 8 confirmed RPV re-entries, DGM found 7. In 1 case (Figure 2, right panel, case 36), DGM detected an additional loop at the LPV. For 1 other case (Figure 2, right panel, case 41) the re-entry pattern traveled between the RPVs around the inferior RPV.

Of the 3 LPV cases, DGM did not detect any correct diagnoses. In 2 cases (Figure 2, right panel, cases 43 and 44) an additional loop around the MV was found, and 1 case (Figure 2, right panel, case 45) remained uninterpretable.

Thus, overall, for the macro-re-entry categories, DGM was correct in 21 of 24 cases or 87.5% of cases.

Double-loop re-entry. Apart from the single-loop re-entries, double-loop re-entries were also diagnosed by the gold standard. Of those, 5 of 6 double-loop re-entries were a combination of 2 macro-re-entrant circuits, whereas 1 was a combination of macro-re-entry and localized re-entry. DGM correctly diagnosed 5 of 6. One example of such a pattern in the RA, shown in Figure 5 (case 50). The left column shows re-entry around IVC and CTI, identified by the HDAM+EM+ablation procedure. For that case, DGM correctly identified the double-loop around IVC and CTI, and those 2 loops can be clearly seen in the right column (Figure 5). In 1 of 6 cases (Figure 2, right panel, case 47), DGM missed a macro-re-entrant MV circuit. However, ablation at MV did not change AT, and roof ablation did restore sinus rhythm. Nonetheless, this case was reported as wrongly diagnosed by DGM and hence was not counted.

ACCURACY OF HDAM COMPARED TO THAT OF THE GOLD STANDARD. To compare HDAM diagnosis results to gold standard results, the authors refer the reader to the additional information found in Strisciuglio et al. (4) and in Figure 2 where HDAM+EM+ablation, and HDAM and DGM are represented. First, HDAM interpretation by the experts resulted in a score of 13 of 13 for the centrifugal patterns (both the focal [3] as well as the passive septal centrifugal activation patterns from right-sided AT [10]). Second, the performance of the correct diagnosis for single, localized reentries dropped to 2 of 10 cases for HDAM. For 5 of 10 cases, the representation of the AT on the HDA map was uninterpretable for the experts. In 2 of 10 cases, an additional circuit around MV was seen. In 1 of 10 cases, HDAM resulted in the interpretation of a CTI-dependent flutter instead of the HDAM+EM+ablation confirmed localized re-entry.

Third, in the single loop macro-re-entries, a CTI-dependent flutter was diagnosed correctly. Also, 5 of 10 MV were correctly identified with HDAM. In the other 5 out of 10 cases, where HDAM+EM+ablation confirmed a MV, the HDAM interpretation resulted in a double-loop diagnosis (Figure 2, right panel, second column, second column). RPV. Also out of 8 RPVs, HDAM interpretation was successful in 5 cases, including case 41 (Figure 2, right panel), where the re-entrant pattern was confirmed between the RPV, circling around the inferior RPV. For the 3 other cases, again, an additional loop was seen on the HDA maps. Of the 3 LPVs, 1 was correctly identified, whereas 2 had an additional loop around the MV.

Finally, 6 double-loop re-entries confirmed by HDAM+EM+ablation were also found with the HDA maps. In total, HDA maps interpretation led to 33 of 51 correctly diagnosed cases. Notably, 5 of 51 cases were not (univocally) interpretable and are shown in Figure 2, right panel with gray boxes.

STATISTICS. A statistical test was carried out to see if results (38 of 51 correct diagnoses) significantly outperformed HDAM (33 of 51 correct diagnoses). The McNemar test gave a p value of 0.1133. Thus, we concluded on the basis of that test's results that the difference between both methods is not significant; however, with 38 of 51 compared to 33 of 51 correct diagnoses, DGM has a trend toward improvement.

DISCUSSION

MAIN FINDINGS. This study applied the novel methodology DGM to complex AT cases. Results showed that DGM can automatically identify the correct mechanism and location of left and right ATs and many outperform HDA alone, although these differences did not reach statistical significance in this study (Central Illustration).

DGM. The correct diagnosis of the AT mechanism and location is pivotal for a targeted and successful ablation. The use of multielectrodes mapping catheters enables the creation of highly detailed high-density maps; however, in the presence of scars and fractionated electrograms (EGMs), a wrong annotation of the LAT renders difficult interpretation of the LAT color-coded maps, and only the more experienced operators may reach the correct diagnosis. DGM is a novel approach to analyze the atrial excitation during AT. DGM creates from the LAT map a directed network where each measured point is a node of the network. Then, based on the LAT of each single node, DGM detects the most probable circuit of propagation and therefore automatically identifies the mechanism

CENTRAL ILLUSTRATION **Diagnostic Accuracy of DGM and HDAM for Complex Atrial Tachycardias**

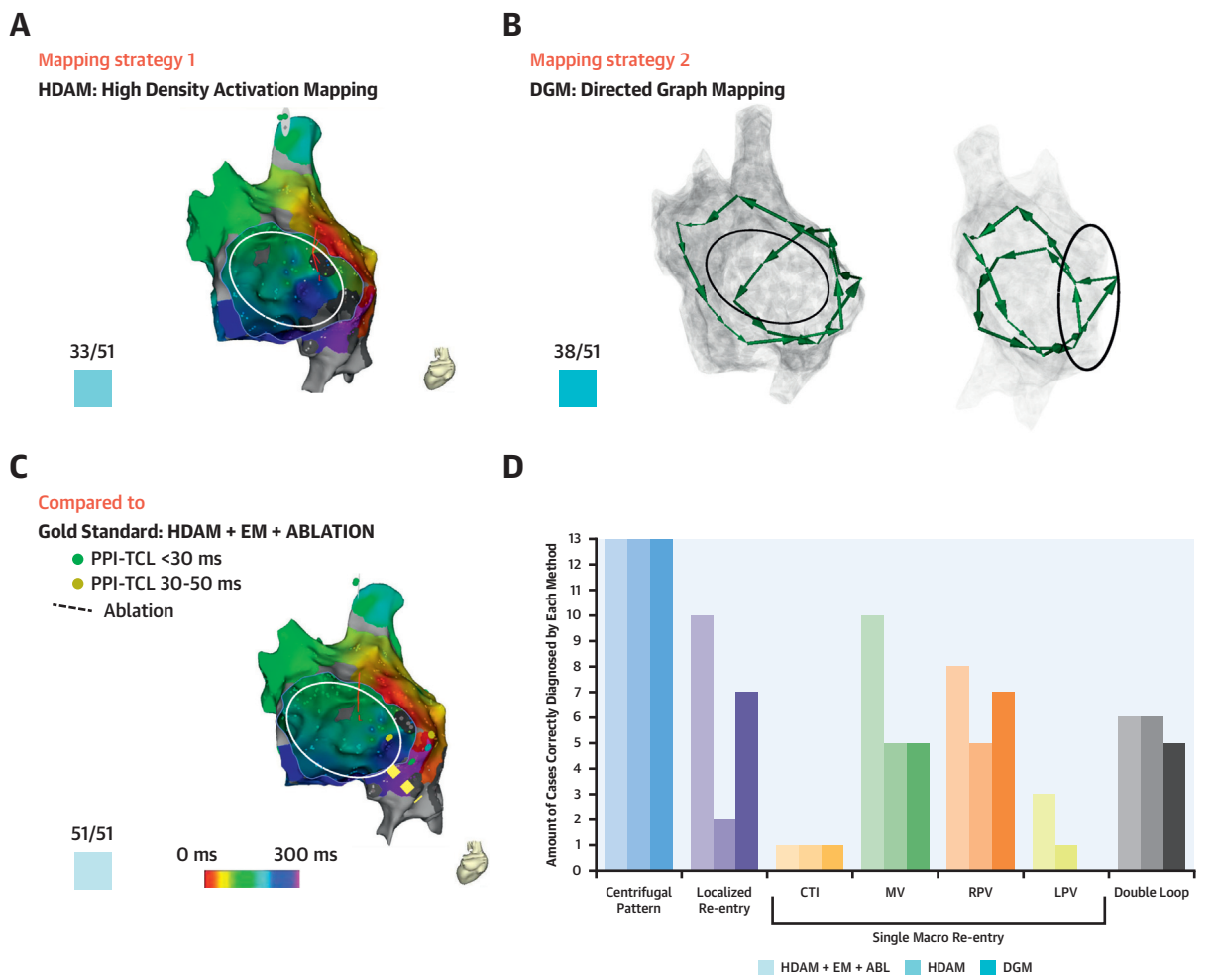

Van Nieuwenhuyse, E. et al. J Am Coll Cardiol EP. 2021;7(7):936–49.

The diagnostic accuracy of DGM on complex atrial tachycardias, compared to the one of HDAM and the gold standard: HDAM + EM + ABL. In this study, the diagnostic accuracy of automated and operator independent directed graph-mapping (DGM) was compared to the accuracy of HDAM. An illustrative case of HDAM is shown in **A**. In **B**, the same representative case was shown with the automated circuits pointed out by DGM. Both were then compared to the gold standard, **C**, which is the three step process of HDAM in combination with entrainment maneuvers and successful ablation leading to sinus rhythm or a different atrial tachycardias. The diagnostic accuracy for different types of atrial tachycardia is shown in **D**. In total, 51 cases were evaluated. Out of these 51 cases, DGM correctly diagnosed 38 cases compared to 33 cases for HDAM. For clearness, this AT was diagnosed by both HDAM and DGM as a double loop reentry around the tricuspid and the inferior vena cava and was confirmed by the gold standard. CTI =cavotricuspid isthmus; DGM = directed graph-mapping; EM = entrainment mapping; HDAM = high density activation mapping; LPV = left pulmonary vein; MV = mitral valve; PPI-TCL = post-pacing interval- tachycardia cycle length; RPV = right pulmonary vein.

and location of the AT. The whole process, from the construction of the network to the identification of the loop source of the AT is based on a mathematical algorithm and is therefore operator-independent. Conversely, the LAT color-coded maps have some disadvantages: 1) the color code is based on the arbitrary setting of the window of interest; 2) the wrong LAT annotation may determine the presence of multiple "early" and "late" areas on the map where the identification of the correct mechanism is not possible; and 3) the maps can be interpreted differently by different operators. When these situations occur, the manual editing of the LAT annotation and the analysis of single EGMs is the solution; however, this is a time consuming task. As the authors have shown in previous work (5), DGM is able to overcome

the wrongly annotated LAT points, and therefore, the editing of the LAT map is not needed. The reason is because DGM not only takes into account local properties of the LATs but takes into account the global picture of the LATs. By optimization of the phase variance and the correct representation of the cardiac excitation pattern with the directed graph, the algorithm became less prone to wrongly annotated signals as they are filtered out. The network will tend to overcome the problems seen in HDA maps as the true mechanism will be found due to the global properties of the network and not some single, wrongly annotated electrograms. Moreover, the DGM analysis is fast and it takes less than 1 minute to detect the correct mechanism, which is represented as a collective of connected directed arrows creating a macro- or micro-loop, or as directed arrows pointing outward from a local source. In previous work (5), DGM reliably detected functional or anatomical re-entry and focal activity in in-silico (ventricular) models. Additionally in the clinical setting of 31 cases of regular AT (also retrospective analysis), it has been demonstrated to be effective in identifying the correct AT mechanism and the site of ablation. In the present study, DGM was tested in a larger setting of complex ATs where its diagnostic accuracy was proved to be comparable with that of HDAM analysis by experts.

SEMIAUTOMATIC MAPPING SYSTEMS FOR IDENTIFICATION OF AT MECHANISMS AND LOCATIONS. The HDAM may be misleading due to the presence of very low voltage and fractionated electrograms whose LAT is often incorrectly annotated, and in these cases we can have 3 scenarios: 1) a wrong interpretation of the maps and therefore a wrong and unsuccessful ablation target; 2) the maps are considered completely uninterpretable and the operator can thus decide to re-map the AT, which prolongs the procedure-time; and 3) the maps can be differently interpreted by different EP physicians, and only the most experienced EP can find the correct diagnosis. These unfortunate scenarios, which highlight the pitfalls of the current mapping systems, have triggered the interest in developing new algorithms and systems to render the ablation of ATs more elegantly. Another computational method was developed to identify the AT mechanism and location through the assessment of cycle length coverage on chamber scale and local level (11). However, its efficacy was proven only in 20 simulated AT scenarios and 3 clinical cases. It would be interesting to compare this approach with that of DGM.

DOUBLE LOOP RE-ENTRY. One of the current drawbacks of DGM is that it tends to find a double-loop, whereas one of the circuits is in fact a passive circuit. As can be found in **Figure 2**, right panel, this is the case for 7 ATs. If DGM can distinguish the passive loop from the active loop, this could lead to an improvement of almost 14%. Current ongoing research in the present authors' group shows that, in simulations, the lowest variance loops tends to be the driving source. However, in the addition of noise and due to the discrete nature of the annotated electrodes in current AT cases, this was not the case. Upon further study and addition of novel algorithms, DGM may be improved to distinguish between passive and active loops in real AT settings. However, in case there is a common isthmus, one can also suggest to always ablate both circuits, if possible through the common isthmus, as the passive circuit could become an active circuit after ablation of the active circuit.

CLINICAL IMPLICATION. The present study demonstrates that the use of DGM in the clinical setting of right and left ATs could be beneficial. The study demonstrated that DGM has a diagnostic accuracy similar to the interpretation of HDA maps' by experts; however, it has the advantage of being independent from the operators experience and interpretation. This is the first tool that is completely automatic and operator-independent as it is based on mathematical algorithms that enable reaching the correct diagnosis of the AT mechanism and location within one minute. Therefore, DGM represents a unique tool to standardize AT ablation procedures, as operator experience will not be an influencing factor. If this tool would be integrated into a mapping system, it would give the opportunity to save time in order to increase the number of procedures as DGM gives an interpretation within a minute, whereas manual interpretation can take up to 15 minutes. Beyond the encouraging results provided so far, further improvements of the DGM tool are desired to add value to clinical practice: 1) an automatic visual suggestion of sites where to perform EM; and 2) an automatic visual suggestion of the successful ablation site. Furthermore in the near future, new features will be added to the DGM tool in order to use it also for other cardiac arrhythmias such as atrial fibrillation and ventricular tachycardias.

STUDY LIMITATIONS. Further studies in a larger population are needed to validate the current findings, as different operators and different mapping systems with different algorithms could have led to different results. Second, the directed network relies on the annotation of the activation times (Wavefront Annotation, Biosense Webster). Even though previous research (5) shows that the DG tool remains stable

with the addition of (Gaussian) noise for the detection of the correct re-entrant circuit, it is not shown in the current study how the automated diagnosis of these ATs is affected by the correctness of the LAT annotation system. Therefore, it is of crucial importance to further test and improve the DGM tool and add LAT annotation to the software itself in order to verify the robustness of DGM regardless of the type of LAT annotation used. Third, double-loop reentries and misleading focal sources next to a line of block will have to be studied thoroughly before DGM will be able to tackle the EM+ablation phase of ablation procedures. However, in the current study, the goal was to evaluate the accuracy of DGM compared to the HDAM phase of the process, and for that, it succeeded.

CONCLUSIONS

DGM is an automatic, fast, and operator-independent tool to identify the AT mechanism and location and it could be a valuable addition to current mapping technologies upon integration in these available mapping systems.

FUNDING SUPPORT AND AUTHOR DISCLOSURES

Dr. Lorenzo is an employee of Biosense Webster. Dr. Goedgebeur is funded with a research grant of the Research Foundation Flanders/Fonds voor Wetenschappelijk Onderzoek (FWO). Dr. Strisciuglio is supported by a research grant from the Cardiopath PhD program. Dr. el Haddad is a consultant for Biosense Webster. Dr. Duytschaever is a consultant for Biosense Webster. All other authors have reported that they have no relationships relevant to the contents of this paper to disclose.

ADDRESS FOR CORRESPONDENCE: Ms. Enid Van Nieuwenhuyse, Department of Physics and Astronomy, Ghent University, Krijgslaan 281, De Sterre, S9, 9000 Gent, Belgium. E-mail: enid.vannieuwenhuyse@ugent.be.

PERSPECTIVES

COMPETENCY IN MEDICAL KNOWLEDGE 1: The current study showed that DGM provides an operator-independent and automatic tool to identify sources of complex AT. The high-density activation mapping leading to successful ablation in combination with EM can be fastened and automated upon integration of DGM in the available mapping technologies. Even in the prior states of its development, DGM competes with state-of-the-art technologies. In further research, we will aim to develop a mapping strategy to optimize presented results and even push the software to the replacement of EM, overcoming operator dependent ablation and enhance successful ablation procedures for (complex) ATs.

COMPETENCY IN MEDICAL KNOWLEDGE 2: This paper shows that it is possible to automatically identify the AT circuit with a similar success rate as a manual interpretation of HDAM by an expert EP. Including this feature in current mapping systems can save time during the procedure by eliminating the analysis of HDAM.

TRANSLATIONAL OUTLOOK: Upon improving DGM by automatically determining the dominant loop when 2 circuits are present, DGM can become a very reliable technique to automatically detect the source and the location of an AT completely automatically making entrainment mapping almost redundant. If this feature would be integrated in the latest mapping software, DGM can show the circuit immediately after the mapping is done. DGM would be robust and operator independent, and therefore possibly reduce the amount of ablation points needed.

REFERENCES

1. I. Deisenhofer H, Estner B, Zrenner J, et al. Left atrial tachycardia after circumferential pulmonary vein ablation for atrial fibrillation: incidence, electrophysiological characteristics, and results of radiofrequency ablation. Europace 2006;8:573–82.

2. Jaïs P, Sanders L-F, Hsu M, et al. Flutter localized to the anterior left atrium after catheter ablation of atrial fibrillation. J Cardiovasc Electrophysiol 2006;17:279–85.

3. Patel AM, d'Avila A, Neuzil P, et al. Atrial tachycardia after ablation of persistent atrial fibrillation: identification of the critical isthmus with a combination of multielectrode activation mapping and targeted entrainment mapping. Circ Arrhythm Electrophysiol 2008;1:14–22.

4. Strisciuglio T, Vandersickel N, Lorenzo G, et al. A prospective evaluation of entrainment mapping as an adjunct to new generations high-density activation mapping systems of left atrial tachycardias. Heart Rhythm 2020;17:211–9.

5. Vandersickel N, Van Nieuwnhuyse E, Van Cleemput N, Goedgebeur J, et al. Directed networks as a novel way to describe and analyze cardiac excitation: directed graph mapping. Front Physiol 2019;10:1138.

6. Anter E, Duytschaever M, Shen C, et al. Activation mapping with integration of vector and velocity information improves the ability to identify the mechanism and location of complex scar-related atrial tachycardias. Circ Arrhythm Electrophysiol 2018;11:e006536.

7. Vandersickel N, Van Nieuwenhuyse E, Panfilov AV. Detection of rotational activity in cardiac electrophysiology; 2018. PCT/EP2018/082799.

8. Sanders P, Hocini M, Jais P, et al. Characterization of focal atrial tachycardia using high-density mapping. J Am Coll Cardiol 2005;46:2088–99.

9. Jais P, Matsuo S, Knecht S, et al. A deductive mapping strategy for atrial tachycardia following atrial fibrillation ablation: importance of localized reentry. J Cardiovasc Electrophysiol 2009;20:480–91.

10. Dong J, Zrenner B, Schreieck J, et al. Catheter ablation of left atrial focal tachycardia guided by electroanatomic mapping and new insights into interatrial electrical conduction. Heart Rhythm 2005;2:578–91.

11. Oesterlein TG, Loewe A, Get Lenis, et al. Automatic identification of re-entry mechanisms and critical sites during atrial tachycardia by analyzing areas of activity. IEEE Trans. Biomed. Eng 2018;65:2334–44.

KEY WORDS atrial tachycardia, catheter ablation, DGM, directed graph-mapping, network theory

APPENDIX For supplemental figures, please see the online version of this paper.